THE JOURNAL OF PHYSICAL CHEMISTRY B

Article

pubs.acs.org/JPCB

Nanoparticle Assembly on Topographical Polymer Templates: Effects of Spin Rate, Nanoparticle Size, Ligand, and Concentration

Mariela J. Pavan, Elina Ploshnik, and Roy Shenhar*

Institute of Chemistry and The Center for Nanoscience and Nanotechnology, The Hebrew University of Jerusalem, Jerusalem, 91904, Israel

Supporting Information

ABSTRACT: The ability to assemble nanoparticles (NPs) into desired patterns in a controlled fashion is crucial for the study of collective properties and for the fabrication of a variety of NP-based devices. Drying-mediated assembly directed by a template provides a facile route for organizing NPs in predefined patterns. We utilize the branched topographical landscapes displayed by partially crystallized poly(ethylene glycol) (PEG) films as a generic template for studying the drying-mediated organization of dodecanethiol- and polystyrene thiol-protected gold NPs (Au-DT and Au-PS), and explore the combined effects of NP size and ligand, concentration, and spin rate on the distribution of NPs inside the channels. We show how NP concentration and the spin rate applied during NP deposition can be used to influence the tendency of NPs either to fill the channel uniformly or to localize near the channel edges, explain the important role of the enhanced aggregation tendency of larger NPs on the resulting morphologies, and demonstrate how this tendency can be tuned by the proper choice of ligands. The different effects are explained in the context of possible scenarios of drying-mediated assembly by analyzing the relevant interactions and forces acting on the NPs during solvent evaporation.

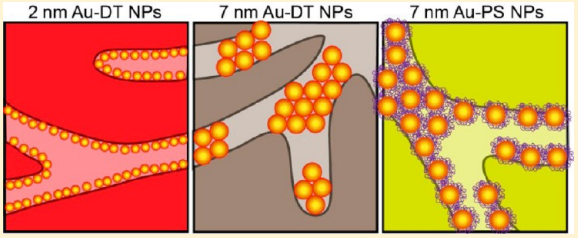

INTRODUCTION

Metal and semiconductor nanoparticles (NPs) have been in the focus of interest in the past few decades due to their unique optical, electronic, magnetic, and catalytic properties, which lead to novel applications.[1−7] Since the collective properties of assembled nanoparticles strongly depend on the morphology of the assembly,[8−12] the creation of certain sophisticated NP-based devices requires the development of techniques for controlling NP organization.

Drying-mediated assembly provides one of the simplest procedures for generating two-dimensional (2D) NP arrangements,[13] but the ability to control the patterning process and its resulting morphology is usually complicated. Considerable improvement is often obtained by using a template to guide the nanoparticle organization. For instance, chemically patterned substrates created thin films of microphase-separated block copolymers provide versatile templates for this purpose.[14−16]

Topographical templates offer an excellent alternative to chemical patterning for guiding NP assembly.[17,18] Initially, partially immersed NPs dragged by the receding, three-phase contact line of the solvent are forced by capillary forces into the trench when the solvent passes over it (Figure 1a). Solvent trapped inside the channels is pinned to the step edges of the trench, and this pinning combined with the continuous evaporation of the solvent leads to deformation of the liquid surface. This gives rise to convective flow, which acts on immersed nanoparticles and directs them toward the pinning sites (Figure 1b).[19−21] Later on, capillary forces between *partially* immersed NPs and the trenches wall direct the NPs to the walls (Figure 1c).[22,23] These forces are long range and usually overcome the forces associated with Brownian motion. Additional factors that influence the organization of NPs inside the channels relate to interparticle interactions. Immersion capillary forces between NPs promote NP aggregation, and formed aggregates later act as pinning sites for the solvent during its evaporation, leading to convective flow that directs more NPs toward the aggregate and thus increases its size (Figure 1d).[21,24] As we shall see below, interparticle interactions can be controlled to a certain extent by the choice of the NP ligands, with marked effect on the NP distribution inside the channels.

In this paper, we explore the drying-mediated assembly of NPs on topographical templates afforded by semicrystalline polymers in ultrathin films. Such films feature branched arrays of channels, which, after being filled with NPs, may lead to applications in sensing, catalysis, electronics, and optics.[25−35] More important for this paper, however, is the fact that semicrystalline polymers provide a versatile platform for the extremely facile creation of topographical landscapes, where morphological parameters such as channel and branching densities can be easily controlled by changing the preparation conditions of the films (e.g., film thickness, temperature, and duration of heating).[36−38] Using this approach, we have recently shown that tuning the NP deposition kinetics to

Received: September 7, 2012
Revised: October 25, 2012

   dx.doi.org/10.1021/jp308910w | J. Phys. Chem. B XXXX, XXX, XXX−XXX

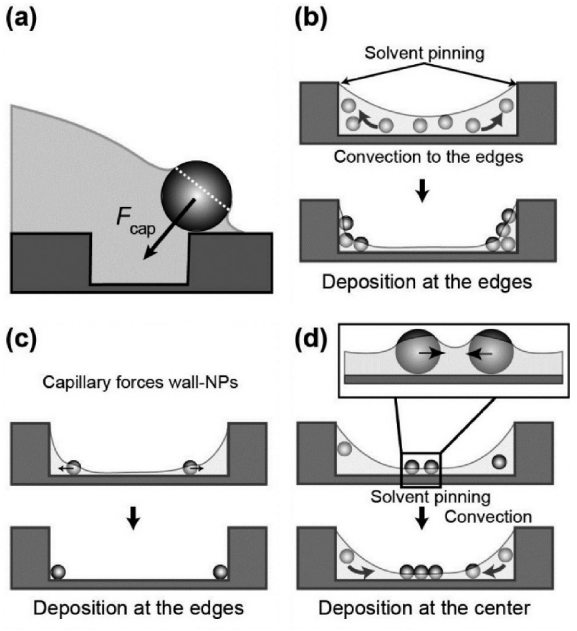

Figure 1. Schematic representation of the various forces acting on the NPs during drying-mediated assembly using topographical templates. (a) Immersion capillary forces directing the NPs to the channel during early stages of the assembly. (b) Convective flow toward the wall caused by solvent pinning to the step edge accompanied by evaporation. (c) Immersion capillary forces between the NP and the wall during the last stages of evaporation. (d) Immersion capillary forces between NPs during the last stages of evaporation and induced convective flow caused by solvent pinning to the aggregate.

match the time scale of the dissolution of the crystalline domains of poly(ethylene glycol) (PEG) in thin films leads to novel, hyperbranched nanoparticle arrays.[36] Here we employ semicrystalline PEG films as generic topographical templates for studying drying-mediated NP assembly, and focus on fast nanoparticle patterning that is achieved by spin coating. We describe a few model cases and show how the spin rate, NP concentration, size, and ligand chemistry can be used to control the distribution of NPs inside the channels.

EXPERIMENTAL SECTION

Materials. Poly(ethylene glycol) (PEG), M_n 56 kg mol^{-1}, polydispersity (M_w/M_n) 1.14 (according to gel permeation chromatography (GPC) analysis in chloroform against polystyrene standards), was purchased from Merck. Chloroauric acid ($HAuCl_4 \cdot 3H_2O$, Acros Organics), sodium borohydride, tetra-*n*-octylammonium bromide (TOAB, Acros Organics), *n*-butyllithium (Acros Organics), and *n*-dodecanethiol (Fluka) were used as received. Styrene (Fluka) and propylene sulfide (Acros) were distilled twice from calcium hydride under high vacuum conditions. *sec*-Butyllithium was synthesized from *sec*-butyl chloride and lithium wires under argon atmosphere. All solvents used were analytical reagent grade. Tetrahydrofuran (THF) was dried with Na/benzophenone and then with *n*-butyllitium before distillation into the reaction flask. Chloroform was kept over molecular sieves before use. Silicon wafers with native oxide layer were purchased from University Wafer, and were cleaned with either a piranha solution or a bath of concentrated sulfuric acid–NoChromix (Godax Laboratories).

Synthesis. PS-SH (M_n 7.2 kDa, PDI 1.22, determined by GPC against PS standards) was synthesized by living anionic polymerization in tetrahydrofuran (THF) at −78 °C under high vacuum conditions. Polymerization of styrene was initiated by *sec*-butyllithium and allowed to proceed for 0.5 h. Polystyryl anions were then titrated by propylene sulfide, after which the sulfide ends were protonated by acidic methanol. The resulting polymer was purified three times by precipitation in methanol.

Dodecanethiol-stabilized gold nanoparticles, 2.0 ± 0.5 nm in diameter (sizes measured from transmission electron microscopy images, see Supporting Information, Figure S1), termed "2 nm Au-DT NPs", were synthesized according to the phase transfer method developed by Brust et al.[39] Au-DT NPs with a diameter of 6.8 ± 1.0 nm, termed "7 nm Au-DT NPs", were synthesized from the 2 nm NPs by the growth method developed by Miyake and co-workers,[40] where the solvent-free, 2 nm Au-DT NPs were heated under nitrogen at heating rate of 2.4 °C/min to 200 °C and maintained at this temperature for 30 min before being air-cooled to room temperature. The NPs were purified at least three times by precipitation in ethanol before use. Au-PS NPs of 7.2 ± 0.9 nm, termed "7 nm Au-PS NPs", were synthesized by ligand exchange of 7 nm Au-DT NPs with thiolated polystyrene (PS-SH) in THF. The NPs were dispersed in toluene and purified by centrifugation with methanol as antisolvent. The procedure was repeated several times until white turbidity was nearly undetectable. Then, two cycles of centrifugation with toluene/hexane were performed.

Characterization. Thermal gravimetry analysis (TGA) was performed on a Metler-Toledo TGA/DSC 1 analyzer, measuring weight loss under nitrogen flow between 30 and 700 °C at a heating rate of 10 °C/min. Dynamic light scattering (DLS) measurements were performed on a Nano-ZS Zetasizer (Malvern UK) on dilute NP solutions prepared in the same solvent used for patterning. Atomic force microscopy (AFM) images were recorded on a Dimension 3100 scanning probe microscope with Nanoscope V controller (Veeco, Santa Barbara, USA). High-resolution scanning electron microscopy (HR-SEM) images were acquired with a Sirion microscope (FEI Co.) operating at 3 or 5 kV acceleration voltages. Transmission electron microscopy (TEM) images were taken in a Tecnai T12 G2 Spirit Microscope (FEI Co.) operating at 120 kV.

Sample Preparation. The polymer template was obtained by spin-casting 0.23 wt % chloroform solutions of PEG onto SiOx wafers, resulting in 19–21 nm thick films. The films were heated at 250 °C under vacuum for 12 h, and then cooled to room temperature under vacuum for approximately 1 day.[36] The obtained template morphology consisted of channels typically 40–70 nm wide and 5–15 nm deep (Figure 2).[41]

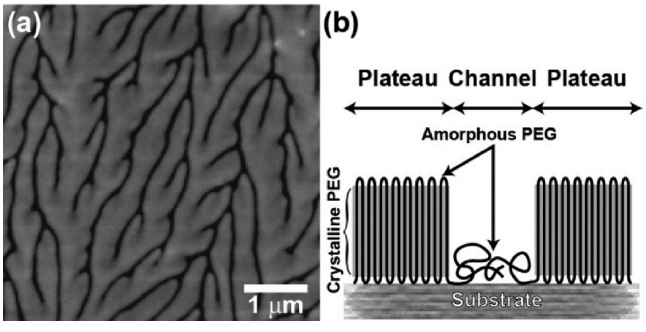

Figure 2. (a) AFM height image of the PEG template and (b) sketch illustrating the polymer chains' disposition in the higher and lower parts of the template. Height contrast is 30 nm.

dx.doi.org/10.1021/jp308910w | J. Phys. Chem. B XXXX, XXX, XXX–XXX

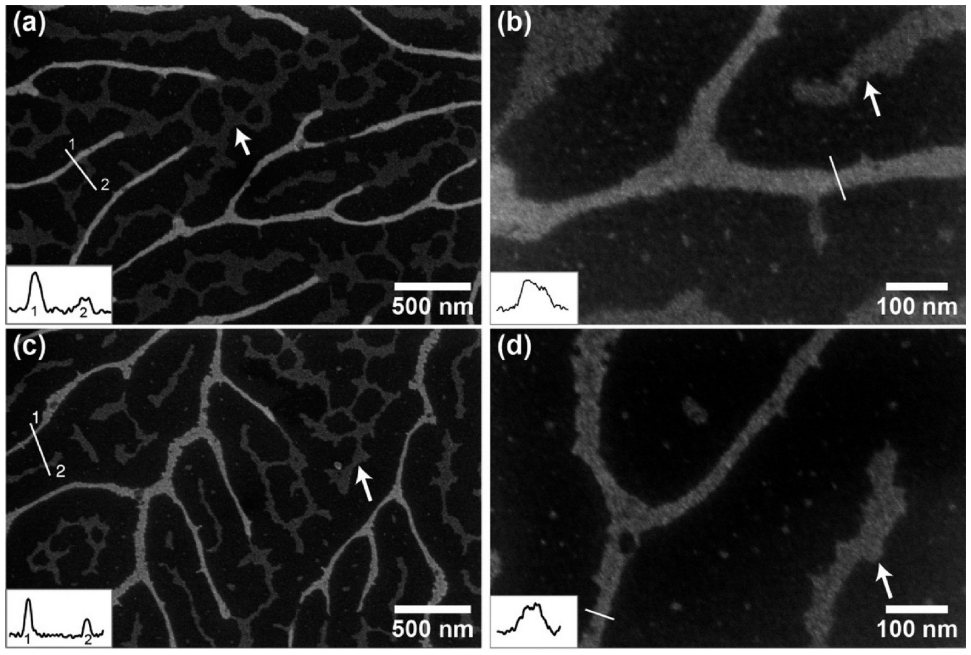

Figure 3. High-concentration case for 2 nm Au-DT NPs: HR-SEM images at two magnifications of a 2 mg/mL solution spin-cast onto PEG template at (a,b) 2000 rpm and (c,d) 8000 rpm. The brightest tone corresponds to NPs located in the channels, and the gray tone corresponds to NP aggregates located on top of the crystalline domains. White arrows point to NP aggregates on top of the plateaus. Insets show intensity profiles measured along the lines in the corresponding images.

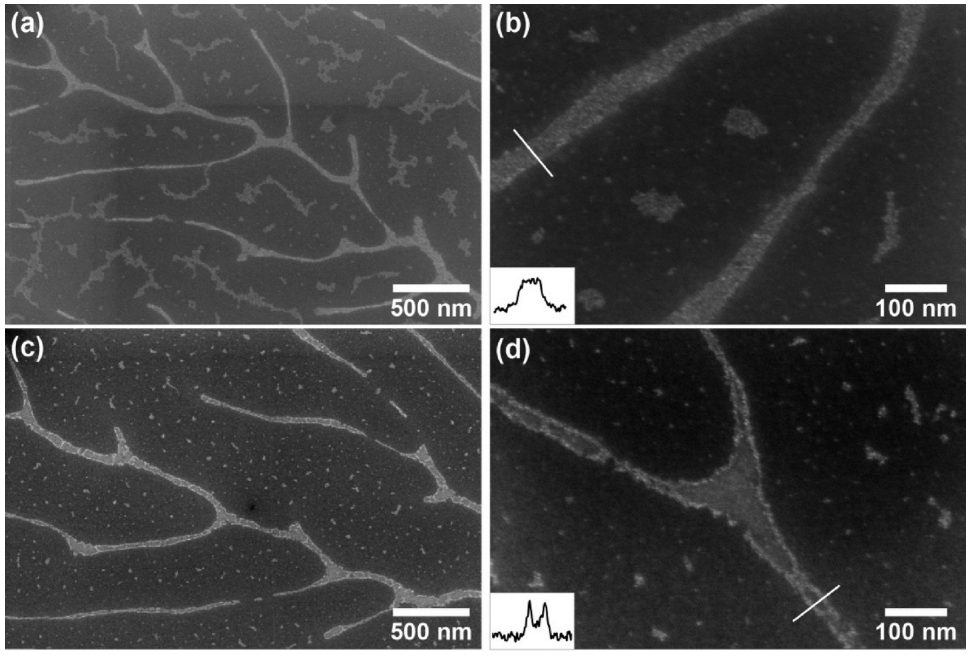

Figure 4. Medium-concentration case for 2 nm Au-DT NPs: HR-SEM images at two magnifications of a 0.8 mg/mL solution spin-cast onto PEG template at (a,b) 2000 rpm and (c,d) 8000 rpm. The brightest, intermediate, and darkest tones in the images correspond to the Au-DT aggregates, portions of the channels that are devoid of NPs, and the crystalline domains, respectively.[42]

Fresh octane solutions of the Au-DT NPs and toluene solutions of the Au-PS NPs were used for patterning. For all NPs, the patterning results of solutions containing different concentrations in the range of 0.5−3.5 mg/mL (determined by UV−vis spectroscopy using an Ocean Optics, Red Tide spectrometer) were examined. The Au-DT and Au-PS solutions were sonicated for 60 and 15 s, respectively, and filtered using a PTFE filter with 0.45 μm pores. In a typical patterning experiment, a droplet of NP solution was spin coated onto the PEG template at either 2000 or 8000 rpm.

RESULTS AND DISCUSSION

Different processes lead to NP ordering on topographical templates, most of them acting at the last stages of drying. Figure 1 shows the main mechanisms leading to different NP distributions inside a channel.

dx.doi.org/10.1021/jp308910w | J. Phys. Chem. B XXXX, XXX, XXX−XXX

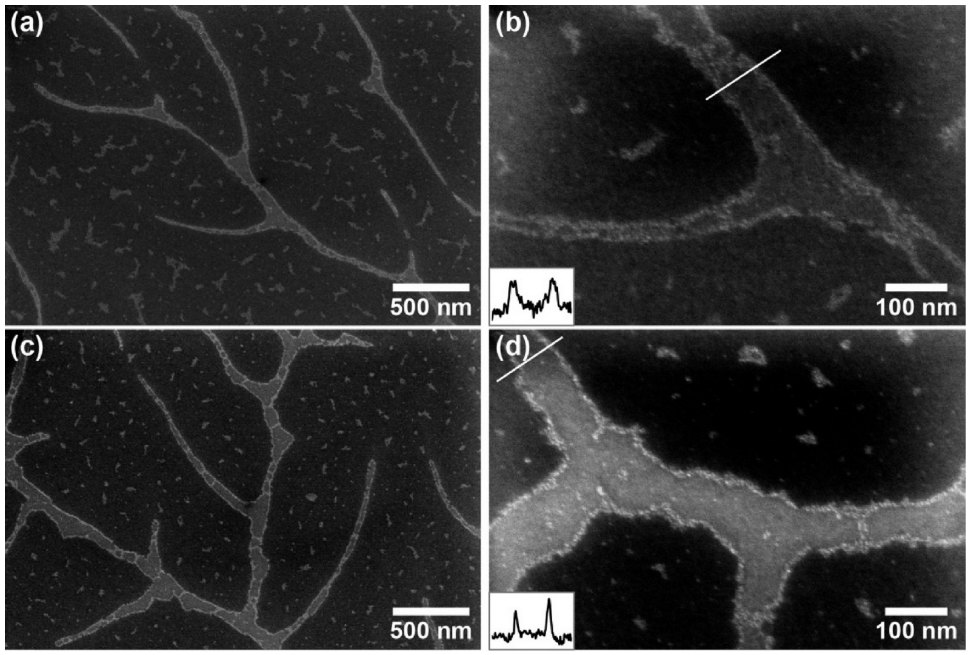

Figure 5. Low-concentration case for 2 nm Au-DT NPs: HR-SEM images at two magnifications of a 0.6 mg/mL solution spin-cast onto PEG template at (a,b) 2000 rpm and (c,d) 8000 rpm.

In this paper, we describe the effect of the NP size on the assembly using dodecanethiol-protected gold NPs (Au-DT) of two different core diameters (2 and 7 nm). Additionally, we study the effect of the NP ligand using NPs of similar core size with two different kinds of ligands: DT and polystyrene thiol (PS-SH). In both studies, the effects of NP concentration and spin rate were explored.

Effect of Concentration and Spin Rate: Assembly of 2 nm Au-DT NPs. The assembly of Au-DT NPs deposited by spin-casting on PEG templates was investigated at three different NP concentrations and two spin rates. When NPs are cast from a concentrated NP solution (2 mg/mL), a large amount of NPs fills the channels (Figure 3). However, a significant amount of NPs is deposited on top of the plateaus as well (appearing as gray aggregates in Figure 3). This amount is reduced for lower concentrations, leading to change in size and shape of these assemblies (Figures 4 and 5). From the brightness contrast it appears that the NP aggregates inside the channels are multilayered compared to the NP assemblies on top of the plateaus. Analysis of AFM images corroborates this observation (see Supporting Information, Figure S3). It should be mentioned that the macroscopic NP distribution on top of the crystalline domains is rather inhomogeneous, where some regions in the same sample exhibit large amount of NPs on the plateaus and others featuring much smaller amount. This behavior is attributed to inhomogeneous solvent evaporation.[13]

A close inspection of the SEM images reveals a strong dependence of the NP distribution inside the channels on the concentration and spin rate. At the highest NP concentration used (2 mg/mL), the NPs distribute nearly uniformly inside the channels (Figure 3), while at the lowest concentration (0.6 mg/mL) the NPs come to rest mostly at the channel edges (Figure 5). In these two cases, no appreciable influence of the spin rate on the qualitative result is observed. For an intermediate NP concentration (0.8 mg/mL), there is a clear correlation between the spin rate and the final NP distribution inside the channels (Figure 4). For the slower spin rate, the distribution of NPs inside the channels is more uniform, while for the higher speed the NPs locate preferentially at the edges of the channels.

To understand the different behaviors noted above, we have to discuss in detail the mechanism that causes the NPs to be trapped in the channels during spin coating. The NP deposition inside the channels results from the combined effect of shear forces (dictated by several parameters such as centrifugal force, viscosity of the solvent, and particle inertia) and capillary forces (determined by the interfacial tensions between all components, the radius of the NP, etc.).[43−45] During spin-casting, centrifugal forces are exerted on the nanoparticles and solvent, which leads to shearing most of the solution away from the substrate. In the thin solution film that remains while spinning continues, the particles and solvent that are not confined inside the channels continue to move in a radial fashion toward the edges of the substrate. As the film thickness becomes comparable to the NP size, immersion capillary forces become dominant in the NP arrangement driving the NPs into the channels (Figure 1a).[17,44]

The final NP distribution inside the channels is dictated by the amount of particles that are trapped in the channels. This amount depends on the number of NPs present in the liquid film in the later stages of drying (i.e., when a thin liquid film still covers the channels). Thus, not only concentrated solutions feature higher number of deposited NPs, but also solutions that have been subjected to slower spin rates. The spin rate may thus be used as a tool to control the distribution of NPs inside the channels.

When a large number of NPs are trapped inside the channels, the outcome is a rather uniform NP distribution across the channel (Figure 6a), caused by NP aggregation across the entire width of the channel. At lower amounts of trapped NPs, however, additional effects have a strong influence on the resulting NP distribution inside the channels. During the last stages of drying, when the solvent is still trapped inside the channels, a meniscus is formed that deepens as the evaporation proceeds. In general, such a scenario may lead to a situation

dx.doi.org/10.1021/jp308910w | J. Phys. Chem. B XXXX, XXX, XXX−XXX

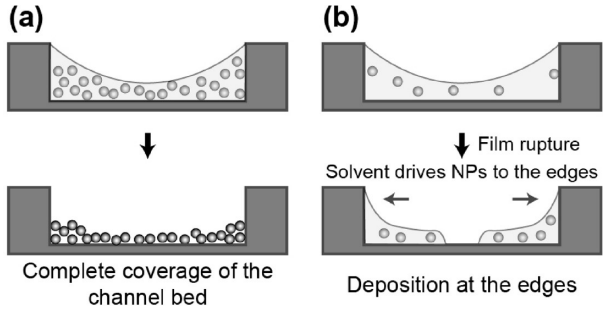

Figure 6. Sketches showing the last stages of drying for a concentrated (a) and dilute (b) NP solution.

where NPs temporarily located at the center of the channel become partially immersed, and immersion capillary forces acting between such particles cause the onset of aggregation at the center of the channel (see Figure 1d). However, for very small NPs, immersion capillary forces between the NPs are relatively weak.[46,47] Additionally, NP nucleation at the center of the channel can only occur when the solvent level becomes thinner than the NP diameter. For small-size NPs, solvent film rupture would occur before immersion capillary forces come into play. Hence, growth of NP clusters at the center of the channel by the combined effect of capillary forces and convection[21,24] is rather improbable. As a result, aggregation near the walls of the channel becomes dominant. We assume that solvent film rupture (Figure 6b)[20,48] is the main cause for this edge decoration, and the contribution of convective flow due to solvent pinning at the step edges before film rupture (Figure 1b)[19,20,49] is marginal. This assumption is based on the fact that the channels are substantially wider than they are deep. Hence, the curvature of the meniscus formed before film rupture occurs is low, leading to very small differences in evaporation rates near the step edges and above the center of the channel. As a result, it is expected that lateral flow of solvent molecules (i.e., convection) would be negligible. Considerable convective forces would develop only after the solvent film ruptures, and assist in conveying the NPs to the edges of the channel. It should be noted that higher spin rates accelerate the rate of evaporation, thus promoting film rupture[20] and deposition of NPs near the channel edges. This conclusion is in accord with our observations regarding the effect of spin rate at medium concentrations (Figure 4), and emphasizes another way by which the spin rate influences the NP distribution in the channels. Finally, capillary action between partially immersed NPs and the channel walls (Figure 1c) could also be largely disregarded, as under the conditions discussed (small NPs at low concentration), film rupture occurs before the NPs become partially immersed.

Effect of NP Core Size: Assembly of 7 nm Au-DT NPs. The NP size is a crucial parameter in NP assembly, since it influences the magnitude of interparticle interaction due to capillary forces (and also van der Waals (vdW) interactions, but these are much less influential[43]). Figures 7–9 show the resulting NP assemblies for three concentrations (2, 1, and 0.5 mg/mL, respectively) and two spin rates (2000 and 8000 rpm). The concentration and spin rate effects are analogous to the ones noted in the case of the smaller NPs. Namely, higher concentrations and lower spin rates lead to higher numbers of deposited NPs and a more uniform distribution of them *across* the channels while lower concentrations and higher spin rates favor deposition of the NPs along the channel edges. In the latter case, unlike with small NPs, the deposition of large NPs near the edges may additionally be facilitated by immersion capillary forces caused by the meniscus formation between the wall and the NP (Figure 1c).

In addition to the similarities with the small NP case, there are several notable differences as well. First, a strong tendency of the NPs to form close packed aggregates is observed, especially for the high concentrations and low spin rate cases. It is important to note that, by and large, extended NP aggregates

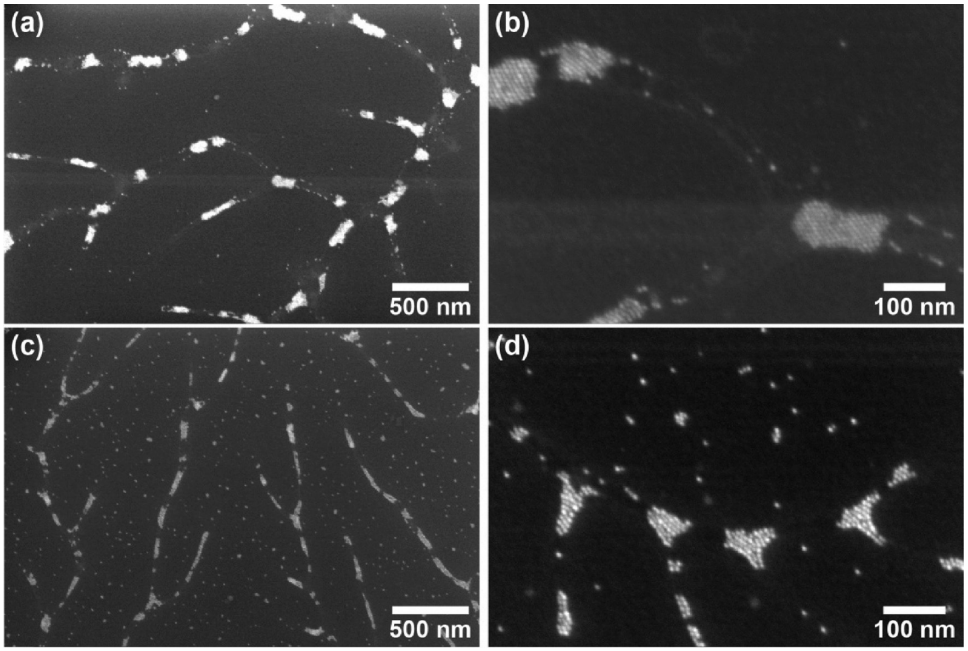

Figure 7. High-concentration case for 7 nm Au-DT NPs: HR-SEM images at two magnifications of a 2 mg/mL solution spin-cast onto PEG template at (a,b) 2000 rpm and (c,d) 8000 rpm.

dx.doi.org/10.1021/jp308910w | J. Phys. Chem. B XXXX, XXX, XXX–XXX

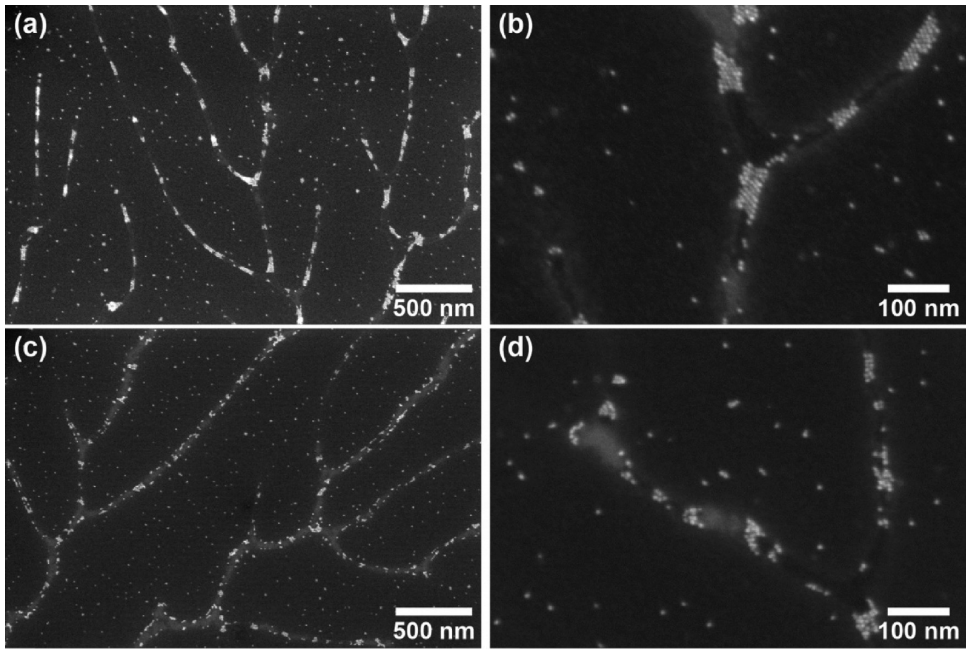

Figure 8. Intermediate-concentration case for 7 nm Au-DT NPs: HR-SEM images at two magnifications of a 1 mg/mL solution spin-cast onto PEG template at (a,b) 2000 rpm and (c,d) 8000 rpm.

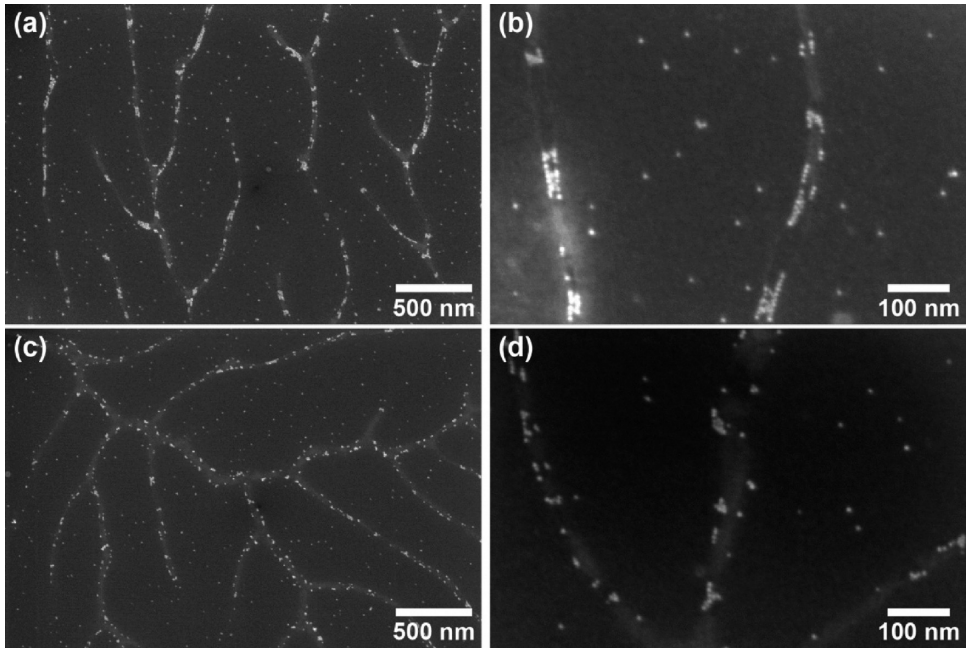

Figure 9. Low-concentration case for 7 nm Au-DT NPs: HR-SEM images at two magnifications of a 0.5 mg/mL solution spin-cast onto PEG template at (a,b) 2000 rpm and (c,d) 8000 rpm.

are not observed on top of the plateaus, indicating that aggregation occurred during the assembly and not already in solution. Second, the distribution of NPs *along* the channels is much less uniform than in the case of the small NPs. This is a direct consequence of the tendency of NPs to aggregate. Third, NP selectivity increases with the NP size, especially for the highest concentrations (compare, for example, Figures 3 and 7).

The increased selectivity of the larger NPs toward the channels agrees with the stronger capillary forces acting on the 7 nm NPs, driving them into the channels. However, the increased selectivity observed for the larger NPs with increasing concentration is somewhat less intuitive. This behavior, together with the higher compatibility of the solvent to the NPs compared to the PEG, implies that the aggregates formed inside the channels retain the solvent longer. Consequently, the solvent dewets the plateaus faster, dragging NPs with it toward the channels.

Another direct ramification of the aggregation tendency of the 7 nm Au-DT NPs is the impeded ability to obtain one-dimensional (1D) and continuous NP decoration of the channel edges. At low concentrations it is obviously impossible, and increasing the concentration triggers 2D aggregation before continuous arrangement of NP at the edges is obtained. As a

dx.doi.org/10.1021/jp308910w | J. Phys. Chem. B XXXX, XXX, XXX−XXX

matter of fact, even obtaining continuous *uniform* filling of the channels is problematic: increasing the concentration to 3.5 mg/mL results in the formation of multilayered, three-dimensional aggregates (Figure 10). This behavior is in line with our explanation regarding the increased selectivity of the larger NPs toward the channels at high concentrations.

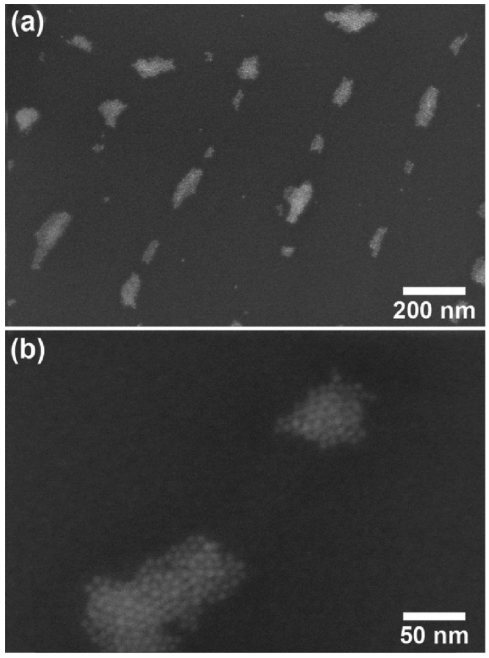

Figure 10. HR-SEM images at two magnifications of a 3.5 mg/mL solution of 7 nm Au-DT NPs spin-cast at 2000 rpm onto PEG template.

The increased aggregation tendency of the large NPs inside the channels indicates that the attractive forces between them are stronger compared to between small NPs. These attractive forces arise mainly from immersion capillary forces.[43] Since immersion capillary forces scale as the square of the NP radius (see Supporting Information), the forces leading to aggregation in the case of the 7 nm NPs are an order of magnitude larger than the ones acting on the 2 nm NPs. In addition, in the course of evaporation, immersion capillary forces start to act earlier on the larger NPs, since these NPs become partially immersed already at higher liquid film thicknesses. As the depth of the channels is on the order of magnitude of the NP size, aggregation of the large NPs at the center of the channel is expected to start before film rupture occurs. Subsequent growth of the aggregate is then facilitated by convective flow (Figure 1d).[21,24] At a very low concentration, however, the number of NPs required for nucleating an aggregate is insufficient. Hence, most NPs are found to localize at the channel edges as small clusters, either dragged by the solvent after film rupture or attracted to the walls by immersion capillary forces.

It is important to note the role of forces acting during the critical stages of early cluster growth at the center of the channel. If cluster growth is slow relative to the rate of evaporation, film rupture occurs before the cluster becomes large enough to pin the solvent to the center of the channel and prevent dewetting. NPs that are conveyed by convective flow to a forming cluster at the center of the channel will adhere to the formed cluster if the net interactions between the NP and the cluster are sufficiently attractive. This enables the cluster to grow rapidly, before evaporation leads to film rupture and dragging NPs toward the walls.

Ligand Effect: Assembly of 7 nm Au-PS NPs. The previous argument about role of additional interactions (i.e., other than capillary forces) between the NPs infers that NP size is not the only parameter dictating whether the resulting morphology of patterned NPs will be aggregates growing from the center of the channels or deposition near the channel walls. Additional interactions, such as van der Waals (vdW), elastic

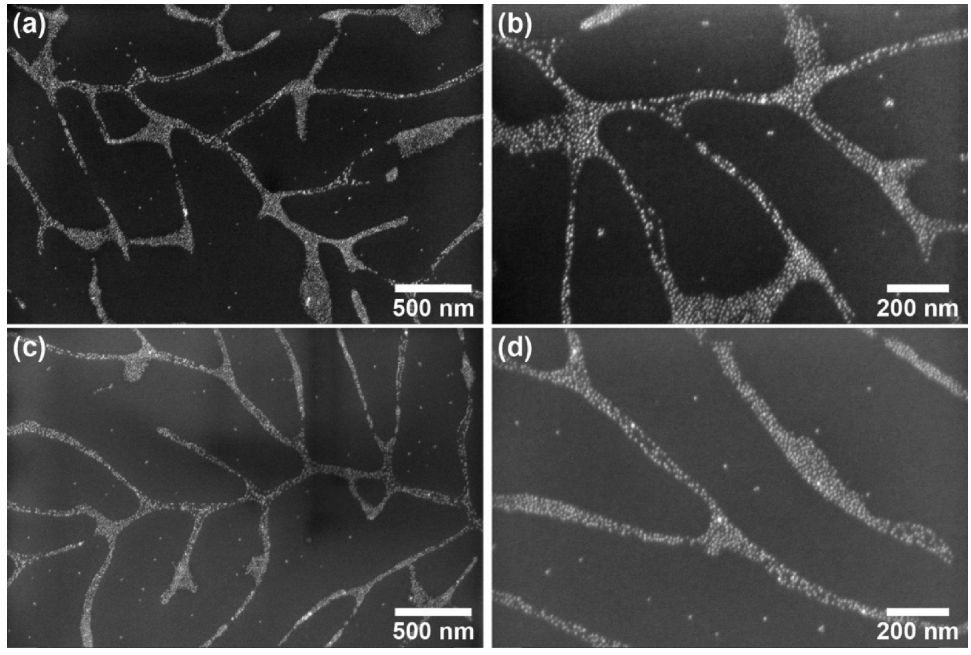

Figure 11. HR-SEM images at two magnifications of a 4 mg/mL solution of 7 nm Au-PS NPs spin-cast onto PEG template at (a,b) 2000 rpm and (c,d) 8000 rpm.

dx.doi.org/10.1021/jp308910w | J. Phys. Chem. B XXXX, XXX, XXX−XXX

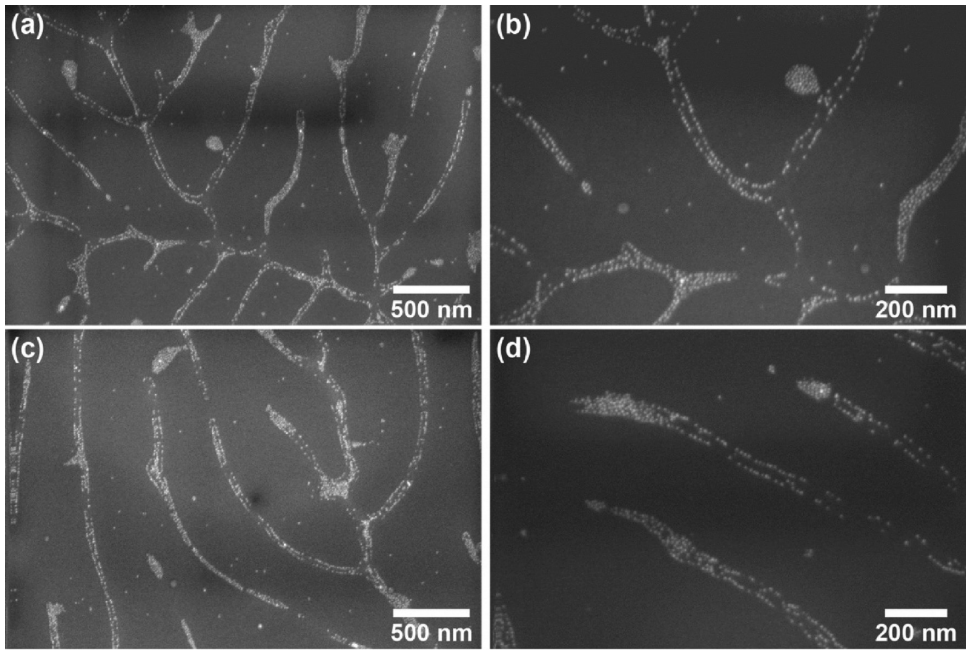

Figure 12. HR-SEM images at two magnifications of a 2 mg/mL solution of 7 nm Au-PS NPs spin-cast onto PEG template at (a,b) 2000 rpm and (c,d) 8000 rpm.

compression, and mixing of ligands between adjacent NPs should also be taken into account. When we compare NPs of the same core diameter, where capillary forces are of similar magnitude, these interactions might dictate the result.

Interparticle interactions are strongly influenced by the nature of the protecting monolayer. Therefore, we decided to study the patterning of NPs of the same core size (7 nm) but different ligands. The ligand influences the magnitude of the total energy of interaction between two NPs by its length, the density of ligands on the surface of the NP, and the interaction between the ligands and the solvent (see Supporting Information for additional details). We concentrated on polystyrene thiol-stabilized gold NPs (Au-PS), synthesized by ligand exchange of the DT in preformed 7 nm Au-DT NPs with polystyrene thiol. To maintain similar miscibility and wetting properties between the NP and the solvent as in Au-DT and octane, the Au-PS NPs were dispersed in toluene (see Supporting Information).

Figures 11 and 12 show the arrangement of Au-PS NPs at different concentrations and spin rates. Similar to the 7 nm Au-DT NPs, a relatively low number of scattered NPs are observed on top of the plateaus formed by the crystalline domains. Interestingly, however, despite the large size of the Au-PS NPs, their assembly behavior *inside* the channels shows similar attributes to the assembly of the small, 2 nm Au-DT NPs. At high concentration, the NPs fill the channels in a considerably more uniform fashion than the corresponding 7 nm Au-DT NPs (Figure 11). As the concentration is lowered, most of the channel areas feature NPs decorating the edges (Figure 12). Isolated aggregates similar to the ones observed for the 7 nm Au-DT NPs (e.g., Figure 7) are not observed.

Considering all the mechanisms discussed above, we analyze the assembly of the 7 nm Au-PS NPs inside the channels as follows. As the size of Au-PS NPs is similar to the size of the large Au-DT NPs and so are the wetting properties with the respective solvents (see Supporting Information for additional details), the magnitude of immersion capillary forces under analogous conditions should be of the same order of magnitude.[17] This suggests that indeed the contributions of the interparticle interactions when the NPs are still immersed (i.e., van der Waals interaction, free energy of mixing of the ligands, and the elastic compression of the ligands) are responsible for the difference in the assembly behavior.[50] Figure 13 shows the interparticle energy curves of the 7 nm

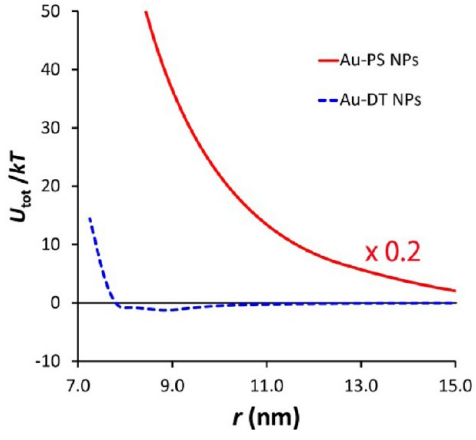

Figure 13. Total interparticle energies calculated for 7 nm Au-DT/octane (blue dashed line) and 7 nm Au-PS/toluene (red smooth line) systems. The curve for Au-PS NPs (red) is multiplied by a factor of 0.02.

Au-DT and 7 nm Au-PS in their respective solvents calculated according to the model developed by Chakrabarti et al. (see Supporting Information for additional details).[50] Although these curves represent a rough estimation, they clearly show that the Au-PS curve is strongly repulsive while the Au-DT curve is slightly attractive with a shallow well.[50−52] In the case of the Au-DT NPs, the vdW interactions contribution at interparticle distances on the order of the NP diameter are considerable, and offset the repulsion arising from ligand

dx.doi.org/10.1021/jp308910w | J. Phys. Chem. B XXXX, XXX, XXX−XXX

mixing and elastic compression. Hence, interparticle interactions between adjacent Au-DT NPs do not pose a considerable barrier for the capillary-force-induced aggregation. In the case of the Au-PS NPs, however, the ligand-induced repulsion dominates over the vdW interactions, hindering the aggregation in this case, as seen in Figure 12.

CONCLUSIONS

The proper tuning of the NP properties and other experimental conditions offers means to control the distribution of deposited nanoparticles in a topographical template. Based on this study, we arrive at the following conclusions:

1. Small, 2 nm diameter NPs either fill the channels uniformly or decorate the edges depending on the NP concentration and spin rate. The latter mode of assembly is apparently dominated by solvent dewetting (film rupture), since immersion capillary forces should be negligible at this size.

2. Increasing the size of the core to 7 nm while maintaining the same ligand coating triggers aggregation due to capillary action between adjacent NPs, since at this size the NPs become partially immersed before film rupture occurs, and the strength of capillary forces increase with NP size. The cluster formed at the center of the channel pins the solvent, which, in combination with the continuing evaporation, leads to convective flow that conveys additional NPs to the growing aggregate.

3. Changing the ligand coating to a polymeric ligand enables to reduce the tendency for aggregation, since it creates effective repulsion between neighboring NPs that may offset the attraction caused by capillary forces. The reasons for this repulsion are the energy associated with ligand mixing and the loss of conformational entropy of the polymeric ligands upon elastic compression.

4. The choice of solvent offers an additional handle for controlling interparticle interactions through its compatibility with the ligands. However, one has to bear in mind that this is limited to the range of solvents that are able to disperse the NPs ($\chi_{solvent/ligand} < 0.5$), otherwise premature aggregation in solution would occur. Additionally, the choice of solvent is limited to solvents that do not dissolve the template.

We believe these findings can be used as guidelines for controlling the assembly of NPs inside topographical templates. These could be useful as the initial stage in the fabrication scheme of functional materials for applications such as conductive transparent electrodes for solar cells and sensory devices. For example, the demonstrated control over the topographical features forming during PEG crystallization[36] could enable tuning the transparency and conductivity of a transparent electrode formed in this way.

ASSOCIATED CONTENT

Supporting Information

TEM characterization of the NPs (Figure S1); TGA analysis of the 7 nm Au-PS NPs (Figure S2); AFM characterization of the 2 nm Au-DT NPs (Figure S3); additional discussions on the choice of solvents, immersion capillary forces, and the estimation of interparticle interactions, including the values of parameters used for this calculation (Table S1). This material is available free of charge via the Internet at http://pubs.acs.org.

AUTHOR INFORMATION

Corresponding Author

*E-mail: roys@huji.ac.il. Tel.: +972-2-6586 311. Fax: +972-2-6585 345.

Notes

The authors declare no competing financial interest.

ACKNOWLEDGMENTS

We thank Daniel Harries and Peter Kralchevsky for stimulating discussions.

REFERENCES

(1) El-Sayed, M. A. *Acc. Chem. Res.* **2001**, *34*, 257.
(2) Daniel, M. C.; Astruc, D. *Chem. Rev.* **2004**, *104*, 293.
(3) Schmid, G.; Simon, U. *Chem. Commun.* **2005**, 697.
(4) Li, R. R.; Dapkus, P. D.; Thompson, M. E.; Jeong, W. G.; Harrison, C.; Chaikin, P. M.; Register, R. A.; Adamson, D. H. *Appl. Phys. Lett.* **2000**, *76*, 1689.
(5) Shipway, A. N.; Katz, E.; Willner, I. *ChemPhysChem* **2000**, *1*, 18.
(6) Murray, C. B.; Kagan, C. R.; Bawendi, M. G. *Annu. Rev. Mater. Sci.* **2000**, *30*, 545.
(7) Park, S. J.; Taton, T. A.; Mirkin, C. A. *Science* **2002**, *295*, 1503.
(8) Thomas, K. G.; Barazzouk, S.; Ipe, B. I.; Joseph, S. T. S.; Kamat, P. V. *J. Phys. Chem. B* **2004**, *108*, 13066.
(9) Xu, K.; Qin, L. D.; Heath, J. R. *Nat. Nanotechnol.* **2009**, *4*, 368.
(10) Pileni, M. P. *Acc. Chem. Res.* **2007**, *40*, 685.
(11) Nie, Z. H.; Fava, D.; Kumacheva, E.; Zou, S.; Walker, G. C.; Rubinstein, M. *Nat. Mater.* **2007**, *6*, 609.
(12) Jain, P. K.; Eustis, S.; El-Sayed, M. A. *J. Phys. Chem. B* **2006**, *110*, 18243.
(13) Rabani, E.; Reichman, D. R.; Geissler, P. L.; Brus, L. E. *Nature* **2003**, *426*, 271.
(14) Shenhar, R.; Jeoung, E.; Srivastava, S.; Norsten, T. B.; Rotello, V. M. *Adv. Mater.* **2005**, *17*, 2206.
(15) Zehner, R. W.; Lopes, W. A.; Morkved, T. L.; Jaeger, H.; Sita, L. R. *Langmuir* **1998**, *14*, 241.
(16) Pavan, M. J.; Shenhar, R. *J. Mater. Chem.* **2011**, *21*, 2028.
(17) Cui, Y.; Bjork, M. T.; Liddle, J. A.; Sonnichsen, C.; Boussert, B.; Alivisatos, A. P. *Nano Lett.* **2004**, *4*, 1093.
(18) Xia, Y. N.; Rogers, J. A.; Paul, K. E.; Whitesides, G. M. *Chem. Rev.* **1999**, *99*, 1823.
(19) Deegan, R. D.; Bakajin, O.; Dupont, T. F.; Huber, G.; Nagel, S. R.; Witten, T. A. *Nature* **1997**, *389*, 827.
(20) Dimitrov, A. S.; Nagayama, K. *Langmuir* **1996**, *12*, 1303.
(21) Denkov, N. D.; Velev, O. D.; Kralchevsky, P. A.; Ivanov, I. B.; Yoshimura, H.; Nagayama, K. *Langmuir* **1992**, *8*, 3183.
(22) Paunov, V. N.; Kralchevsky, P. A.; Denkov, N. D.; Ivanov, I. B.; Nagayama, K. *Colloids Surf.* **1992**, *67*, 119.
(23) Gordon, M. J.; Peyrade, D. *Appl. Phys. Lett.* **2006**, *89*, 053112.
(24) Denkov, N. D.; Velev, O. D.; Kralchevsky, P. A.; Ivanov, I. B.; Yoshimura, H.; Nagayama, K. *Nature* **1993**, *361*, 26.
(25) Sun, H. Z.; Wei, H. T.; Zhang, H.; Ning, Y.; Tang, Y.; Zhai, F.; Yang, B. *Langmuir* **2011**, *27*, 1136.
(26) Cheng, M. F.; Fang, J. H.; Cao, M.; Jin, Y. L. *J. Nanosci. Nanotechnol.* **2010**, *10*, 7451.
(27) Gao, P.; Zhang, M.; Hou, H.; Mao, Q. *Mater. Res. Bull.* **2008**, *43*, 531.
(28) Sukhanova, A.; Volkov, Y.; Rogach, A. L.; Baranov, A. V.; Susha, A. S.; Klinov, D.; Oleinikov, V.; Cohen, J. H. M.; Nabiev, I. *Nanotechnology* **2007**, *18*, 185602.
(29) Hu, Y.; Pan, N.; Zhang, K.; Wang, Z.; Hu, H.; Wang, X. *Phys. Status Solidi (A)* **2007**, *204*, 3398.
(30) Sukhanova, A.; Baranov, A. V.; Perova, T. S.; Cohen, J. H. M.; Nabiev, I. *Angew. Chem., Int. Ed.* **2006**, *45*, 2048.
(31) Xu, X.; Jia, J.; Yang, X.; Dong, S. *Langmuir* **2010**, *26*, 7627.
(32) Jing, C. Y.; Fang, Y. *J. Colloid Interface Sci.* **2007**, *314*, 46.

(33) Wen, X.; Xie, Y.-T.; Mak, W. C.; Cheung, K. Y.; Li, X.-Y.; Renneberg, R.; Yang, S. *Langmuir* **2006**, *22*, 4836.
(34) Fairbanks, M. S.; McCarthy, D. N.; Scott, S. A.; Brown, S. A.; Taylor, R. P. *Nanotechnology* **2011**, *22*.
(35) Samavati, H.; Hajimiri, A.; Shahani, A. R.; Nasserbakht, G. N.; Lee, T. H. *IEEE J. Solid-State Circuits* **1998**, *33*, 2035.
(36) Pavan, M. J.; Shenhar, R. *J. Mater. Chem.* **2010**, *20*, 1247.
(37) Reiter, G.; Sommer, J. U. *Phys. Rev. Lett.* **1998**, *80*, 3771.
(38) Massa, M. V.; Dalnoki-Veress, K.; Forrest, J. A. *Eur. Phys. J. E* **2003**, *11*, 191.
(39) Brust, M.; Walker, M.; Bethell, D.; Schiffrin, D. J.; Whyman, R. *J. Chem. Soc., Chem. Commun.* **1994**, 801.
(40) Teranishi, T.; Hasegawa, S.; Shimizu, T.; Miyake, M. *Adv. Mater.* **2001**, *13*, 1699.
(41) Channel width was measured at middle height.
(42) The lower part of the template appears brighter due to emission of secondary electrons from the underlying substrate.
(43) Liddle, J. A.; Cui, Y.; Alivisatos, P. *J. Vac. Sci. Technol., B* **2004**, *22*, 3409.
(44) Zhao, Y.; Marshall, J. S. *Phys. Fluids* **2008**, *20*, 043302.
(45) Darling, S. B. *Surf. Sci.* **2007**, *601*, 2555.
(46) Danov, K. D.; Pouligny, B.; Kralchevsky, P. A. *Langmuir* **2001**, *17*, 6599.
(47) Kralchevsky, P. A.; Nagayama, K. In *Particles at Fluids Interfaces and Membranes: Attachment of Colloid Particles and Proteins to Interfaces and Formation of Two-Dimensional Arrays*; Elsevier Science B.V.: Amsterdam, 2001.
(48) Yamaki, M.; Higo, J.; Nagayama, K. *Langmuir* **1995**, *11*, 2975.
(49) Su, G.; Guo, Q.; Palmer, R. E. *Langmuir* **2003**, *19*, 9669.
(50) Khan, S. J.; Pierce, F.; Sorensen, C. M.; Chakrabarti, A. *Langmuir* **2009**, *25*, 13861.
(51) Goubet, N.; Richardi, J.; Albouy, P.-A.; Pileni, M.-P. *Adv. Funct. Mater.* **2011**, *21*, 2693.
(52) Goubet, N.; Richardi, J.; Albouy, P. A.; Pileni, M. P. *J. Phys. Chem. Lett.* **2011**, *2*, 417.